

Satellite imagery for bauxite mine waste mapping in the frame of the m4mining project.

Evlampia Kouzeli¹, Konstantinos Nikolakopoulos¹, Olga Sykioti², Saeid Asadzadeh³, Friederike Koerting⁴, Daniel Schlöpfer⁵

¹ GIS and Remote Sensing Lab, Department of Geology, University of Patras, Patras 26504, Greece;
knikolakop@upatras.gr (K.N.); e.kouzeli@upatras.gr (E.K.)

² National Observatory of Athens, Institute for Astronomy, Astrophysics, Space Applications and Remote Sensing,
Athens Greece; sykioti@noa.gr (O.S.)

³ Helmholtz Centre Potsdam, GFZ German Research Centre for Geosciences, 14473, Potsdam, Germany;
saeid@gfz-potsdam.de (S.A.)

⁴ Norsk Elektro Optikk AS—HySpex Division, Østensjøveit 34, 0667 Oslo, Norway; friederike@neo.no (F.K.)

⁵ ReSe Applications LLC Langeggweg 3 9500 Wil Switzerland daniel@rese-apps.com (D.S.)

Keywords: Sentinel-2, WV3, EnMap, SAM, Mine Wastes

Abstract

Mine wastes, including tailings (the by-products of mineral processing), are subject to weathering, leading to environmental issues. During the last decades, the traditional, cost-effective, and time-consuming field methods are replaced by remote sensing (RS), which is based on multispectral and hyperspectral data for mining monitoring. In this case study, we investigate the waste material of an inactive bauxite mine in Greece. We select satellite data with different spatial and spectral resolutions to map mining wastes.

The goal of this study is to classify mine waste based on mineral indicators using the Spectral Angle Mapper (SAM) with hyperspectral and multispectral data. Moreover, spectral signatures of minerals from two different spectral libraries are used, namely the United States Geological Survey (USGS) Spectral Library and the Jet Propulsion Laboratory (JPL) Spectral Library. The spectral signatures related to the objective of this study are resampled to the Environmental Mapping and Analysis Program (EnMap), Sentinel-2, and World View 3 (WV3) spectral bands.

We present the results of all datasets. We also describe each satellite sensor's capability to map and discriminate the specified mineral indicators and refer to their detected differences. This study demonstrates that RS exhibits varying levels of effectiveness based on data spatial and spectral resolution to identify and map mineral indicators.

1. Introduction

The mining industry is one of the most critical parts of the worldwide economy. Raw materials such as bauxite, coal, pyrite, and many others are significant for a day- to - day living. However, waste materials such as tailings are generated from mining and processing, contributing to environmental contamination. The primary constituents of bauxite are iron oxides/hydroxides, aluminum oxides/hydroxides, clay, and sulfate minerals. Despite that, the interest in tailings characterization is not only for environmental reasons but also for significant raw material recovery (Mujabar et al., 2019; Kasmaeeyazdi et al., 2018).

With the widely used per-pixel Spectral Angle Mapping (SAM) technique, the angle between the spectrum of the spectral signature and the spectrum of the pixel to be classified (Wakasa et al, 2020) is calculated. In literature, hyperspectral (Kayet et al., 2018; Davies and Calvin, 2017) and multispectral (Moghtaderi et al., 2020; Wakasa et al, 2020) data are analysed in the field of geology and mining, including, among other methods, SAM. For example, mine waste classification is conducted using SAM on Sentinel-2 data in the Fe-Mn mine in Odisha, India, with a 95.8 % overall accuracy (Guglietta et al., 2020). Bauxite deposits are mapped using SAM on ASTER imagery in the wider area of Saudi Arabia (Mujabar and Dajkumar, 2018). Iron ore minerals (hematite, goethite, and desert) are also mapped using SAM on Hyperion data with a 77% overall accuracy (Kayet et al., 2018).

In this study, we focus on mapping key minerals for bauxite mine wastes using different types of multispectral and hyperspectral imagery. The endmembers are retrieved from two different spectral libraries (USGS and JPL) while SAM is applied to give insights into each sensor's capability to detect the key spectral indicators of bauxite residues in wastes and see how effectively they can be mapped using remote sensing.

2. Data and methods

The study area (Figure 1) is the Arkoudotrypa inactive bauxite mine located in Greece's Parnassos–Ghiona unit. Satellite data with diverse spatial resolutions ranging from 30 to 3.7m (EnMap, Sentinel-2, and WV3-SWIR correspondingly) are used.

Six minerals are selected as anticipated to be present in the study area, namely diaspore, goethite, hematite, kaolinite, muscovite, and calcite. These minerals are selected to map low-temperature alteration and weathering. The USGS and JPL spectral libraries are used to retrieve the spectral signatures (named here after endmembers which are shown in Table 1, Figure 2, and Figure 3) of diaspore, goethite, hematite, muscovite, kaolinite, and calcite. The initial spectra are resampled to EnMap, Sentinel-2, and WV3-SWIR spectral bands. The spectral signature of diaspore is not available in the JPL library. Despite boehmite being anticipated in the study area, its spectral signature was not available in either the USGS or JPL library.



Figure 1. Study area: Inactive bauxite mine in the broader Delphi area, Central Greece (the figure on the left shows the prefecture boundaries outlined by a black line and the municipality borders marked with a red line. The yellow pin is the exact location of the mine, and the figure on the right indicates the mine based on Google Earth pro).

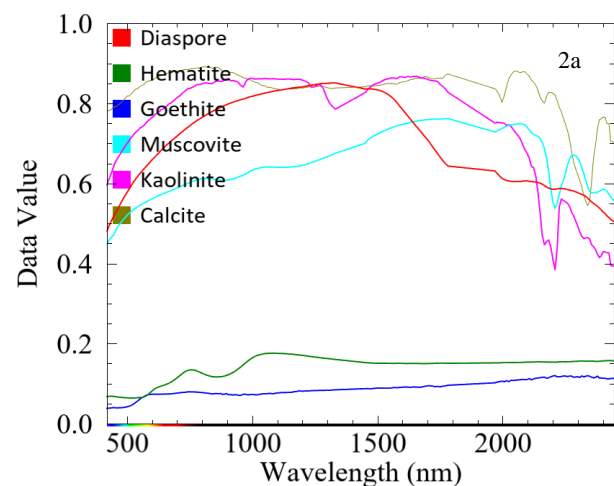
The USGS and JPL spectral signatures of each of the six minerals are evaluated using the SAM algorithm, revealing the endmembers with the lowest detected spectral angle threshold. Each mineral's endmember is used in the SAM analysis with EnMap, Sentinel-2, and WV3-SWIR data to identify which one results in the smallest spectral angle. Since the study area is characterized by fine-grained minerals, grain size is taken into consideration in conjunction with the spectral purity of the sample, while the presence/absence of the contaminants is defined by the spectral purity. For this reason, all available spectral signatures of each mineral in each library corresponding to relatively pure samples with fine to medium grain size were taken into consideration. In addition, based on the aforementioned criteria, the spectral signature of each mineral presenting the minimum detected spectral angle is finally retained.

For the purpose of this study, the atmospherically corrected EnMap data (acquired 2024/06/19) VNIR-SWIR (224 spectral bands) are provided by the Helmholtz Centre Potsdam - GFZ German Research Centre for Geosciences (GFZ). The EnMap spectral bands 131-135 (1342.82-1390.48nm) are set as bad bands and excluded from the analysis. A Sentinel-2 Level 2A VNIR-SWIR image (12 spectral bands) is used (European Space Agency), acquired on 2024/06/26. Finally, a dataset of WV3-SWIR (8 spectral bands) is also used (2024/01/06-SWIR). The WV3-SWIR data are atmospherically corrected by ReSe Applications. The spatial resolutions of the EnMap, Sentinel-2, and WV3-SWIR data are 30m, 10m, and 3.7m, respectively. Each

scene is cropped to the mine area extent. The pixel and endmember reflectance values vary between 0 and 1.

Mineral	Spectrum Title
Diaspore	Diaspore_HS416.1B_ASDFRb Not Available
Hematite	Hematite_HS45.3_ASDFRb Hematite alpha Fe ₂ O ₃ [oxide-nine-medium-o01a]
Goethite	Goethite_HS36.3_BECKb Goethite alpha Fe ³⁺ O(OH) [hydroxide-nine-fine-oh02a]
Muscovite	Muscovite_HS146.1B_ASDFRa Muscovite KAl ₂ (Si ₃ Al)O ₁₀ (OH,F) ₂ [silicate-phyllsilicate-medium-ps16a]
Kaolinite	Kaolinite_GDS11_lt63um_BECKb Kaolinite Al ₂ Si ₂ O ₅ (OH) ₄ [silicate-phyllsilicate-fine-ps01a]
Calcite	Calcite_HS48.3B_BECKa Calcite CaCO ₃ [carbonate-nine-fine-c03a]

Table 1. Description of endmembers in this study. For each mineral in the second column, the first row corresponds to the spectral signature name in the USGS spectral library, and the second row corresponds to the spectral signature name in the JPL spectral library. The spectrum title and information are retrieved from the corresponding ancillary file of each mineral from each spectral library (Meerdink et al, 2019; Kokaly et al., 2017, and Baldrige et al., 2009).



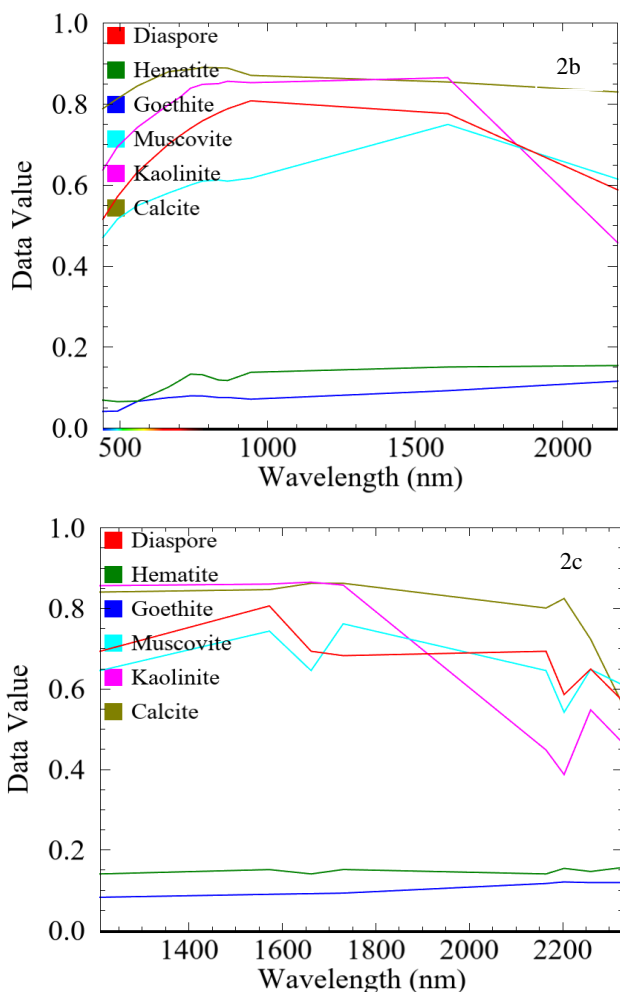


Figure 2. Mineral spectral signatures in this study, (a) are retrieved from the USGS spectral library and are resampled to the EnMap spectral bands; (b) retrieved from the USGS spectral library and are resampled to the Sentinel-2 spectral bands; (c) retrieved from the USGS spectral library and are resampled to the WV3-SWIR spectral bands.

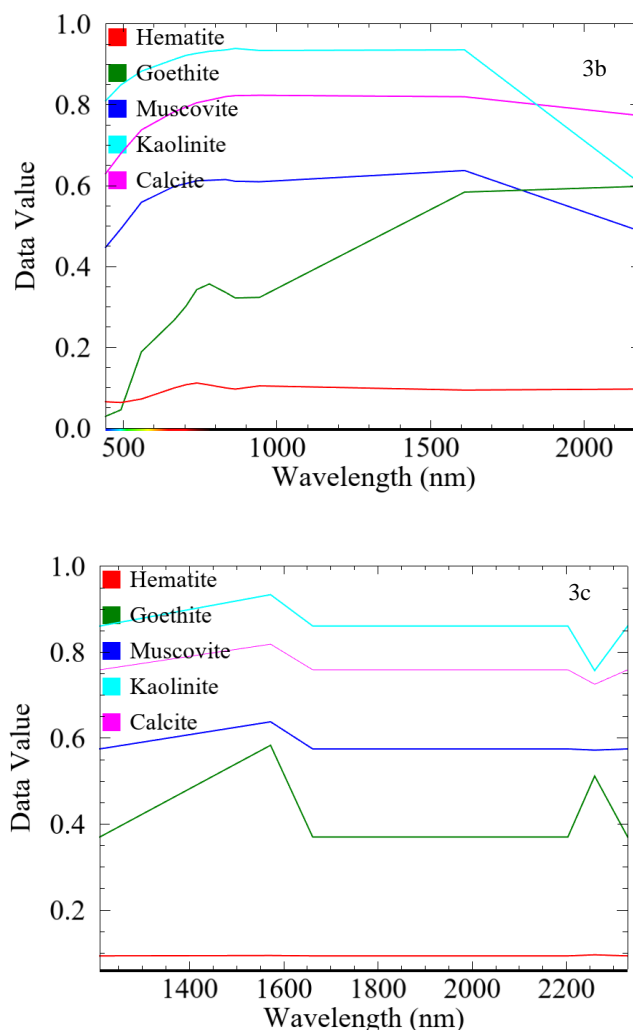
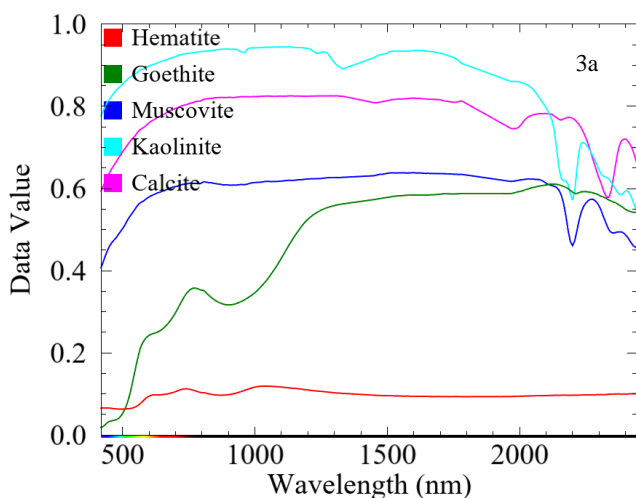


Figure 3. Mineral spectral signatures in this study, (a) are retrieved from the JPL spectral library and are resampled to the EnMap spectral bands; (b) are retrieved from the JPL spectral library and are resampled to the Sentinel-2 spectral bands; (c) are retrieved from the JPL spectral library and are resampled to WV3-SWIR spectral bands.



In the framework of SAM, the spectral vectors of six USGS endmembers and five JPL endmembers are used to calculate their spectral angle with each pixel vector of each dataset. The threshold angle for SAM was set to 0.25 radians for EnMap (USGS and JPL endmember), 0.15 radians and 0.20 radians for Sentinel-2 (USGS & JPL endmembers), and 0.15 radians for WV3-SWIR (USGS and JPL endmembers, respectively).

It is important to note that WV3 lacks the VNIR spectral bands typically used to compute NDVI, which may affect vegetation masking accuracy for this dataset. Since the vegetation in the study area is sparse, it was manually extracted based on the historical imagery of Google Earth Pro and was applied to WV3-SWIR. The 0.25 NDVI threshold was applied to EnMap and Sentinel-2 VNIR-SWIR.

3. Results and discussion

Mineral detection and mapping, utilizing data from sensors like EnMap, Sentinel-2, and WV3 in conjunction with

spectral libraries (e.g., USGS or JPL endmembers), is influenced by several factors that justify the similarities and differences between the results. These factors include the sensor specifications, such as band wavelength position and shape, spectral range, spectral band, spatial resolution, and acquisition date, as well as the inherent physical properties of the samples (e.g., particle size, specific chemistry, and environmental context) from which spectral signatures were derived. Topographical and seasonal variations could also contribute to these influences.

3.1 USGS endmembers

As aforementioned, the angle threshold values with which the minerals are mapped for EnMap, Sentinel-2, and WV3-SWIR are set to 0.25, 0.15, and 0.15 radians, respectively. The classification maps that correspond to the six minerals, showing their spatial distribution concerning the range of the angle threshold, are given in Figures 4 to 9. The following paragraphs describe the range of angle threshold values within which the minerals are detectable.

All minerals are mapped with EnMap (Figures 4a, 5a, 6a, 7a, 8a, and 9a). Diaspore, hematite, goethite, and muscovite are mapped with Sentinel-2 data, but kaolinite and calcite were hardly detected with Sentinel-2 (Figures 4b, 5b, 6b, 7b, 8b, and 9b). Diaspore, muscovite, and calcite are spatially dominant with WV3-SWIR; however, hematite and kaolinite are hardly detected (Figures 4c, 5c, 7c, 8c, and 9c). Goethite is not mapped with WV3-SWIR data under the predefined angle threshold (Figure 6c).

Diaspore as mapped by the EnMap sensor is detected across the study area with an angle threshold of 0.225-0.25 radians for the majority of the pixels. In Sentinel-2 data, diaspore is also mapped within the study area, mostly with a 0.125-0.175-radian angle threshold. With the same angle threshold as in the Sentinel-2 case, diaspore is mapped by WV3-SWIR. Comparing the spatial distribution of diaspore in each one of the three datasets, a common spatial pattern is observed. However, it must be noted here that the EnMap angle threshold is higher than the corresponding one for Sentinel-2 and WV3-SWIR (Figure 4).

Hematite is classified within the study area using EnMap and Sentinel-2, with angle thresholds of 0.12-0.20 radians and 0.10-0.15 radians, respectively. In WV3-SWIR, hematite appears to be almost absent, which could be due to the lack of VNIR spectral bands, which are important for the diagnostic identification of ferric minerals such as hematite. (Figure 5).

Goethite is also mapped with EnMap data using an angle of 0.225-0.25 radians and is spatially present in the entire study area. On the other hand, it is not mapped with WV3-SWIR due to the absence of VNIR spectral bands as in the case of hematite. Finally, goethite is mapped with Sentinel-2 with a lower angle threshold (0.10-0.125) compared to the EnMap corresponding one (Figure 6).

Concerning muscovite, it seems that this mineral dominates the study area when applying SAM to EnMap with an angle threshold of 0.125-0.20 radians at the middle and an angle threshold of 0.225-0.25 radians at the edge of the study area, which probably indicates less presence of muscovite at borders of the study area. In Sentinel-2, muscovite is mapped with an angle threshold of 0.025-0.125 radians in the center of the study area and an angle threshold of 0.125-0.15 radians at the borders of the study area; however, in WV3-SWIR, muscovite is classified with an angle threshold of

0.125-0.150 but in a lesser spatial extent than EnMap and Sentinel-2 (Figure 7).

Kaolinite is hardly mapped using EnMap, Sentinel-2, and WV3-SWIR. Especially, with Sentinel-2 and WV3-SWIR and a predefined 0.15 angle threshold, kaolinite is almost absent. Kaolinite, as a clay mineral, is anticipated to be detectable in the SWIR spectral region, and its absence probably indicates either its limited presence or that it is spectrally overlapped by muscovite. (Figure 9).

Calcite as mapped by EnMap is sparsely detected within the study area with an angle threshold of 0.20-0.25 radians. It is almost absent in Sentinel-2 while carbonates have diagnostic features in SWIR and long-wave infrared (LWIR). In contrast to Sentinel-2, which has only two SWIR spectral bands, calcite was mapped with the eight WV3-SWIR spectral bands with an angle threshold ranging from 0.025 to 0.15 radians, appears to exhibit a halo pattern, with the highest spectral angle values surrounding the lower values. (Figure 9c).

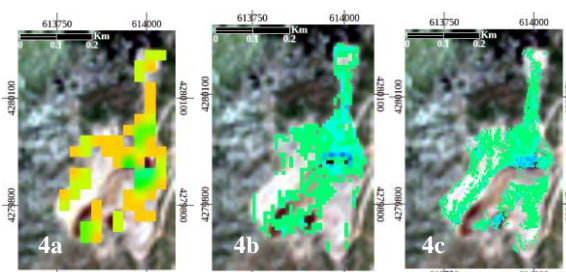


Figure 4. SAM-USGS diaspore classification maps (a) EnMap (2024/06/19); (b) Sentinel-2 (2024/06/26); and (c) WV3-SWIR (2024/01/06). From left to right, the results were displayed for EnMap, Sentinel-2, and WV3-SWIR when the mineral was classified. The background image is the TCI of Sentinel-2 (2024/06/26). Spectral angle values range between 0.00-0.125 are given with purple to light blue colors, 0.125-0.225 with medium to light green colours, and 0.225-0.25 with light orange colour.

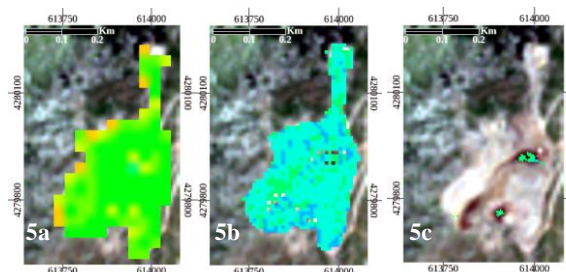


Figure 5. SAM-USGS hematite classification maps (a) EnMap (2024/06/19); (b) Sentinel-2 (2024/06/26); and (c) WV3 (2024/01/06). From left to right, the results were displayed for EnMap, Sentinel-2, and WV3-SWIR when the mineral was classified. The background image is the TCI of Sentinel-2 (2024/06/26). Spectral angle values range between 0.00-0.125 are given with purple to light blue colors, 0.125-0.225 with medium to light green colours, and 0.225-0.25 with light orange colour.

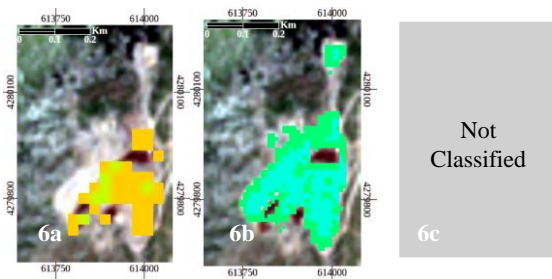


Figure 6. SAM-USGS goethite classification maps (a) EnMap (2024/06/19); (b) Sentinel-2 (2024/06/26); and (c) WV3 (2024/01/06). From left to right, the results were displayed for EnMap, Sentinel-2, and WV3-SWIR when the mineral was classified. The background image is the TCI of Sentinel-2 (2024/06/26). Spectral angle values range between 0.00- 0.125 are given with purple to light blue colors, 0.125-0.225 with medium to light green colours, and 0.225-0.30 with light orange to red colours.

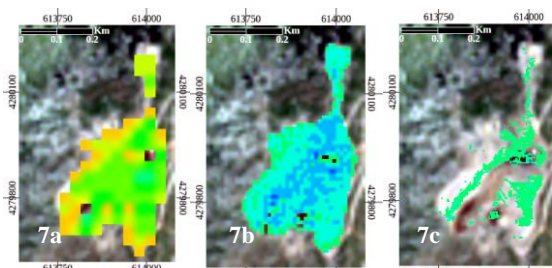


Figure 7. SAM-USGS muscovite classification maps (a) EnMap (2024/06/19); (b) Sentinel-2 (2024/06/26); and (c) WV3-SWIR (2024/01/06). From left to right, the results were displayed for EnMap, Sentinel-2, and WV3-SWIR when the mineral was classified. The background image is the TCI of Sentinel-2 (2024/06/26). Spectral angle values range between 0.00- 0.125 are given with purple to light blue colors, 0.125-0.225 with medium to light green colours, and 0.225-0.25 with light orange colour.

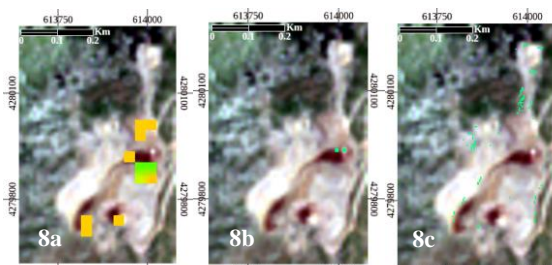


Figure 8. SAM-USGS kaolinite classification maps (a) EnMap (2024/06/19); (b) Sentinel-2 (2024/06/26); and (c) WV3-SWIR (2024/01/06). From left to right, the results were displayed for EnMap, Sentinel-2, and WV3-SWIR when the mineral was classified. The background image is the TCI of Sentinel-2 (2024/06/26). Spectral angle values range between 0.00- 0.125 are given with purple to light blue colors, 0.125-0.225 with medium to light green colours, , and 0.225-0.25 with light orange colour.

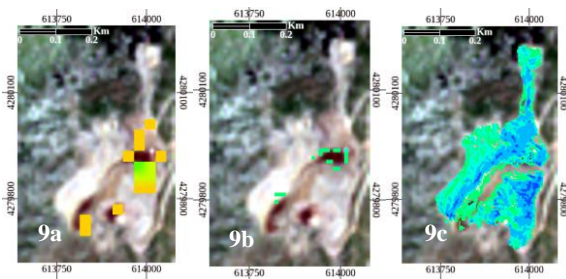


Figure 9. SAM-USGS calcite classification maps (a) EnMap (2024/06/19); (b) Sentinel-2 (2024/06/26); and (c) WV3 (2024/01/06). From left to right, the results were displayed for EnMap, Sentinel-2, and WV3-SWIR when the mineral was classified. The background image is the TCI of Sentinel-2 (2024/06/26). Spectral angle values range between 0.00-0.125 are given with purple to light blue colors, 0.125-0.225 with medium to light green colours, , and 0.225-0.25 with light orange colour.

EnMap and Sentinel-2 hematite and muscovite had the lowest angle thresholds in contrast to diaspore, goethite, kaolinite, and calcite angle thresholds. WV3-SWIR data indicated that calcite is identified with the smallest angle threshold in comparison with diaspore and muscovite.

The grain size and the purity of the endmembers seem to affect the results. The 74-200nm grain size of hematite, goethite, and calcite, and the <5µm grain size of diaspore and muscovite potentially represent better the grain size of the minerals in the study area. Finally, the grain size of kaolinite is less than 63 µm, which resulted in a limited number of mapped pixels in both EnMap and WV3-SWIR data under the 0.15 radians angle thresholds, which is the same for the minerals of each sensor (the 0.15 radians angle threshold is the same for the six minerals for WV3-SWIR).

Among the USGS endmembers only muscovite and calcite are spectrally pure, as indicated by the spectral purity code “a” while diaspore, hematite, goethite, and kaolinite seem spectrally pure but potentially have contaminants that affect the results to some degree, as indicated by the spectral purity code “b”. For instance, with the spectral signature of Hematite_GDS27_BECKa, hematite is not mapped with the Sentinel-2 sensor, as it is anticipated; however, with the Hematite_HS45.3_ASDFRb Hematite is mapped in the study area, indicating that the spectral purity of the endmembers likely affects the results.

Ultimately, it was observed that the angle threshold for the mineral classification exhibits the following trend: EnMap VNIR-SWIR>Sentinel-2 and WV3-SWIR, indicating a higher threshold for EnMap and lower angle thresholds for the Sentinel-2 and WV3-SWIR data.

3.2 JPL endmembers

The SAM algorithm is also tested for mine waste mineral mapping using reference spectra from the JPL spectral library. The angle threshold values for EnMap, Sentinel-2, and WV3-SWIR are 0.25, 0.20, and 0.15 radians, respectively. The classification maps that correspond to the five minerals (hematite, goethite, muscovite, kaolinite, and calcite), showing their spatial distribution concerning the range of the angle threshold, were given in Figures 10 to 14. Using the SAM algorithm, we map all the minerals with EnMap data. All minerals are also mapped with Sentinel-2 apart from goethite; however, hematite and muscovite have the strongest spatial presence. Muscovite, kaolinite, and

calcite are spatially dominant with WV3-SWIR, but hematite and goethite are hardly detected. Muscovite, kaolinite, and calcite are mapped under a 0.125-0.20 angle threshold. The following describes the range of angle threshold values within which the minerals are detectable.

Hematite is classified in the entire study area with EnMap using an angle of 0.175-0.25 radian, with the majority of the pixels presenting 0.225-0.25 angle values. Sentinel-2 data gives a similar spatial pattern to EnMap but with a 0.10-0.20 angle threshold. Hematite with WV3-SWIR data is unclassified under the 0.15 angle threshold, probably due to the absence of VNIR bands (Figure 10).

Goethite is mapped with EnMap data using an angle of 0.20-0.25 radian and was spatially present within the entire study area. On the other hand, goethite is not mapped with Sentinel-2 and WV3-SWIR imagery (Figure 11).

Muscovite is mapped with EnMap data using an angle of 0.175-0.25 radian within the entire study area. In Sentinel-2 and EnMap, muscovite has the same spatial pattern but with a lower angle threshold of 0.10-0.20 radians in Sentinel-2 (Figures 12a and 12b). In WV3-SWIR, muscovite is mapped using an angle threshold of 0.075-0.15 radian and spatially covers a significant portion of the study area (Figure 12).

Kaolinite is mapped with EnMap data at an angle of 0.175-0.25 radian, while in Sentinel-2 it is mapped using an angle of 0.15-0.25 radian. In WV3-SWIR, kaolinite is mapped using an angle threshold of 0.10-0.15 (Figure 13) in a higher spatial extent than EnMap and Sentinel-2.

Calcite was mapped with EnMap and WV3-SWIR data using an angle threshold of 0.20-0.25 and 0.025-0.175 radian, respectively; it spatially covers a significant part of the study area. In Sentinel-2, calcite is mapped using an angle of 0.125-0.200 radian. Finally, in WV3-SWIR, calcite is mapped using an angle threshold of 0.10-0.20 radian in the study area (Figure 14).

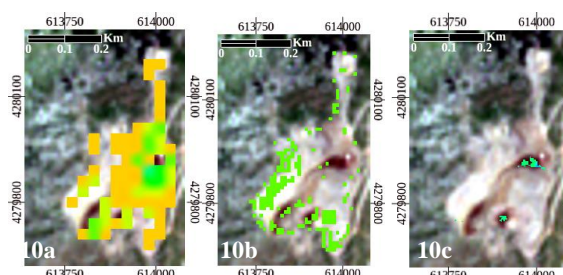


Figure 10. SAM-JPL hematite classification maps (a) EnMap (2024/06/19); (b) Sentinel-2 (2024/06/26); and (c) WV3-SWIR (2024/01/06). From left to right, the results were displayed for EnMap, Sentinel-2, and WV3-SWIR when the mineral was classified. The background image is the TCI of Sentinel-2 (2024/06/26). Spectral angle values range between 0.00- 0.125 are given with purple to light blue colors, 0.125-0.225 with medium to light green colours, , and 0.225-0.25 with light orange colour.

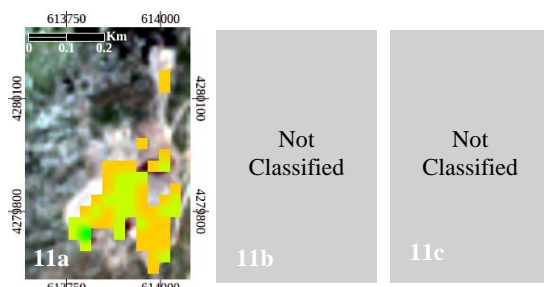


Figure 11. SAM-JPL goethite classification maps (a) EnMap (2024/06/19); (b) Sentinel-2 (2024/06/26); and (c) WV3 (2024/01/06). From left to right, the results were displayed for EnMap, Sentinel-2, and WV3-SWIR when the mineral was classified. The background image is the TCI of Sentinel-2 (2024/06/26). Spectral angle values range between 0.00-0.125 are given with purple to light blue colors, 0.125-0.225 with medium to light green colours, and 0.225-0.25 with light orange colour.

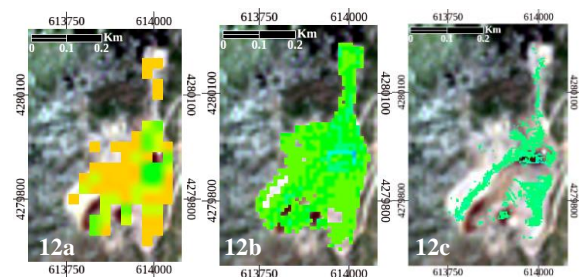


Figure 12. SAM-JPL muscovite classification maps (a) EnMap (2024/06/19); (b) Sentinel-2 (2024/06/26); and (c) WV3-SWIR (2024/01/06). From left to right, the results were displayed for EnMap, Sentinel-2, and WV3-SWIR when the mineral was classified. The background image is the TCI of Sentinel-2 (2024/06/26). Spectral angle values range between 0.00- 0.125 are given with purple to light blue colors, 0.125-0.225 with medium to light green colours, and 0.225-0.25 with light orange colour.

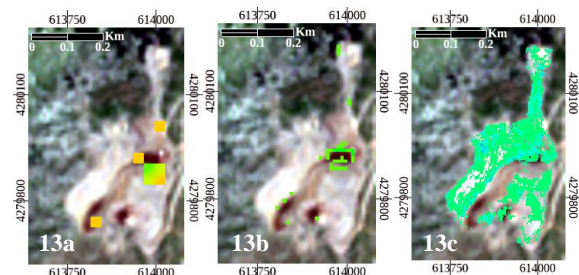


Figure 13. SAM-JPL kaolinite classification maps (a) EnMap (2024/06/19); (b) Sentinel-2 (2024/06/26); and (c) WV3-SWIR (2024/01/06). From left to right, the results were displayed for EnMap, Sentinel-2, and WV3-SWIR when the mineral was classified. The background image is the TCI of Sentinel-2 (2024/06/26). Spectral angle values range between 0.00- 0.125 are given with purple to light blue colors, 0.125-0.225 with medium to light green colours, , and 0.225-0.25 with light orange colour.

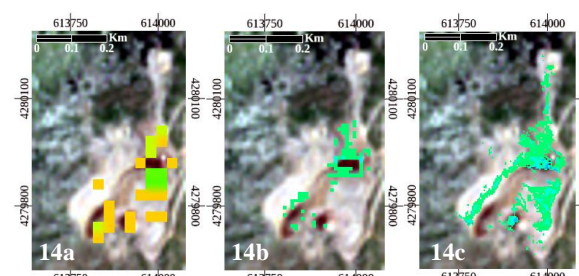


Figure 14. SAM-JPL calcite classification maps (a) EnMap (2024/06/19); (b) Sentinel-2 (2024/06/26); and (c) WV3-SWIR (2024/01/06). From left to right, the results were displayed for EnMap, Sentinel-2, and WV3-SWIR when the mineral was classified. The background image is the TCI of Sentinel-2 (2024/06/26). Spectral angle values range between 0.00- 0.125 are given with purple to light blue

colors, 0.125-0.225 with medium to light green colours, , and 0.225-0.25 with light orange colour.

EnMap hematite, goethite, and muscovite have approximately the same spatial pattern, while WV3-SWIR muscovite and calcite follow almost the same spatial distribution. The 74-125nm grain size of hematite and muscovite and the 0-45µm grain size of goethite, kaolinite, and calcite-potentially represents better the grain size of the minerals in the study area.

At long last, it was observed that the angle threshold for the mineral classification exhibits the following trend: EnMap > Sentinel-2 > WV3-SWIR, indicating a lower angle threshold for WV3-SWIR and higher angle thresholds for EnMap for the JPL spectra library.

4. Conclusions

The objective of the study was to give insights into each sensor's capability to detect key mineral indicators of bauxite mine wastes and see how effectively they can be mapped using remote sensing techniques. In this paper, we present the results of the application of the SAM method using endmembers from two different spectral libraries (USGS, JPL) and data from three different sensors (EnMap, Sentinel-2, and WV3-SWIR) in a pixel-level analysis.

Each mineral's endmember is used in the SAM analysis with the three sensors' data to identify which one results in the smallest spectral angle. For instance, ten different spectral signatures of hematite are used in the SAM analysis, with the signature 'Hematite_HS45.3_ASDFRb' yielding the smallest spectral angle.

USGS endmembers: The fine grain size of the diaspore and muscovite, and the medium grain size of hematite, goethite, and calcite seem to lead to lower angle thresholds. The spectrally pure muscovite and calcite, along with the less spectrally pure diaspore, hematite, goethite, and kaolinite, also yield results with low-angle thresholds. Potentially indicates that the grain size and the spectral purity of the minerals may affect the results.

Considering the angle threshold, the diaspore is better mapped with Sentinel-2 and WV3-SWIR. It is noted that a common 0.125–0.175 radians angle threshold range is attributed to most of Sentinel-2 and WV3-SWIR pixels; hematite is represented better with Sentinel-2 of 0.10-0.15 radians angle threshold range, at this range captures the majority of the pixels of the scene; goethite is also mapped better with Sentinel-2 and a 0.10–0.125 radians angle threshold range, at this range map the bulk of the pixels; a significant number of muscovite pixels are captured with Sentinel-2 and a 0.025-0.15 radians angle threshold range; Even though the spectral signature of the kaolinite in the initial analysis resulted in the lowest angle threshold value among the other kaolinite spectral signatures, it was still hard to map kaolinite in the study area. Kaolinite is restricted to a small number of pixels in the EnMap with a 0.225-0.25 radians angle threshold range, and calcite is mapped with WV3-SWIR and a 0.025-0.15 radians angle threshold range, representing a significant number of the pixels.

JPL endmembers: The fine grain size of the goethite, kaolinite, and calcite, and the medium grain size of hematite and muscovite seem to lead to lower angle thresholds. Goethite, kaolinite, and calcite seem spectrally pure whilst hematite and muscovite exhibit some spectral contamination. Considering the angle threshold, hematite is represented better with Sentinel-2 of 0.10-0.20 radians angle threshold

range, at this range most of the pixels are captured; goethite is mapped with EnMap and a 0.20–0.25 radians angle threshold range; a significant number of muscovite pixels are captured with Sentinel-2 and a 0.10-0.20 radians angle threshold range; kaolinite is mapped with WV3-SWIR and a 0.10-0.15 radians angle threshold range; and calcite is mapped with WV3-SWIR and a 0.025-0.175 radians angle threshold range representing a significant number of the pixels.

Summarizing, under defined angle thresholds, the USGS fine to medium-grained endmembers, either talking about spectrally pure or less spectrally pure endmembers, in conjunction with Sentinel -2, seem to map diaspore, hematite, goethite, and muscovite in the scene with lower angle thresholds, whilst WV3-SWIR seems to map calcite more efficiently. JPL fine-to-medium-grained endmembers in conjunction with EnMap appear to map goethite, while Sentinel-2 is more effective at mapping hematite and muscovite. Additionally, WV3-SWIR maps kaolinite and calcite.

However, the conclusions are based on comparisons with USGS/JPL libraries' spectra where the samples are from other regions (potentially exhibiting characteristics different from the characteristics of those in the study area), which may affect the results.

We also note, in contrast to EnMap and Sentinel-2 summer acquisitions, that WV3-SWIR spectral data reflected winter conditions characterized by a 26° sun elevation, 158.6° sun azimuth, and cloud-free skies. The winter acquisition poses a dark shadow area in WV3-SWIR data where we are unable to map any minerals, either using the USGS or JPL libraries. Shadows created by low illumination might compromise accuracy, possibly leading to both false positive/negative outcomes for WV3-related results. It is recommended to perform the acquisition, if circumstances permit, under conditions of high solar elevation.

However, validation using in-situ data will reveal the effectiveness of SAM and each dataset in mapping and distinguishing the minerals in the study area. Currently, we have gained insights through a visual comparison of the resulting maps. We are currently investigating in-situ sampling, laboratory analyses, and spectral measurements to verify our findings, which is an ongoing work.

Acknowledgements



"m4mining" project is funded by the European Union's Horizon Europe programme under Grant Agreement ID 101091462.

We are thankful to the European Space Agency (ESA) for providing, free of charge, the WV3-SWIR (2024/01/06) data under the accepted project proposal **PP0094982** - M4Mining "Multiscale and Multisensor Remote Sensing Data processing for Mine tailing management" – Case study sites in Greece and in the Republic of Cyprus.

References

Mujabar, P.S., Dajkumar, S., 2019: Mapping of bauxite mineral deposits in the northern region of Saudi Arabia by using Advanced Spaceborne Thermal Emission and Reflection Radiometer satellite data. *Geo-Spatial Information Science* 22, 35–44. doi.org/10.1080/10095020.2018.1530857

Kasmaeeyazdi, S., Mandanici, E., Balomenos, E., Tinti, F., Bonduà, S., Bruno, R., 2021: Mapping of aluminum concentration in bauxite mining residues using Sentinel-2 imagery. *Remote Sensing* 13, 1517. doi.org/10.3390/rs13081517

Wakasa, A., Takeda, T., Marincović, V., Hirose, K., 2020: Jarosite distribution maps based on the Sentinel-2 image band calculations and jarosite abundance analyses in the Bor mining area, Serbia. *Environmental Earth Sciences* 79, 307. doi.org/10.1007/s12665-020-09048-6

Kayet, N., Pathak, K., Chakrabarty, A., Sahoo, S., 2018: Mapping the distribution of iron ore minerals and spatial correlation with environmental variables in hilltop mining areas. *Environ Earth Sci* 77, 308. doi.org/10.1007/s12665-018-7482-7

Davies, G.E., Calvin, W.M., 2017: Mapping acidic mine waste with seasonal airborne hyperspectral imagery at varying spatial scales. *Environ Earth Sci* 76, 432. doi.org/10.1007/s12665-017-6763-x

Moghtaderi, A., Moore, F., Ranjbar, H., 2022: Testing ASTER and Sentinel-2 MSI Images to Discriminate Igneous and Metamorphic Rock Units in the Chadormalu Paleocrater, Central Iran. *Canadian Journal of Remote Sensing* 48, 214–238. doi.org/10.1080/07038992.2021.1997347

Guglietta, D., Belardi, G., Passeri, D., Salvatori, R., Ubaldini, S., Casentini, B., Trapasso, F., 2020: Optimising the management of mining waste by means Sentinel-2 imagery: a case study in Joda West Iron and Manganese Mine (India). *Journal of Sustainable Mining* 19. doi.org/10.46873/2300-3960.1003

European Space Agency (ESA). (2024). Sentinel-2 data from Copernicus Data Space Ecosystem. Copernicus Open Access Hub. <https://dataspace.copernicus.eu>

Meerdink, S.K., Hook, S.J., Roberts, D.A., Abbott, E.A., 2019: The ecostress spectral library version 1.0. *Remote sensing of environment*, 230(111196), 1–8. doi.org/10.1016/j.rse.2019.05.015

Kokaly, R.F., Clark, R.N., Swayze, G.A., Livo, K.R., Hoefen, T.M., Pearson, N.C., Wise, R.A., Benzel, W.M., Lowers, H.A., Driscoll, R.L., Klein, A.J., 2017: USGS Spectral Library Version 7, Data series 1035. doi.org/10.3133/ds1035

Baldrige, A.M., Hook, S.J., Grove, C.I., Rivera, G., 2009: The ASTER Spectral Library Version 2.0. *Remote Sensing of Environment*, 113, 711-715. doi.org/10.1016/j.rse.2008.11.007

Meyer, J.M., Kokaly, R.F., Holley, E., 2022: Hyperspectral remote sensing of white mica: A review of imaging and point-based spectrometer studies for mineral resources, with spectrometer design considerations. *Remote Sensing of Environment* 275, 113000. <https://doi.org/10.1016/j.rse.2022.113000>